

**MASTER M2
UE QUESTIONS D'ACTUALITÉ EN IMMUNOLOGIE
SESSION DE JANVIER 2008**

Durée de l'épreuve : 3 heures.

Le sujet porte sur l'article ci-joint publié en 2006 par Bleul *et al.* (Nature 44, 992-996).

Questions

- 1) Proposer un titre pour l'article et rédiger un résumé (maximum 120 mots) (8 points)
- 2) Expliquer à l'aide d'un diagramme le principe de fonctionnement de la protéine Cre-ERT2. Quel est l'effet du tamoxifène ? Pourquoi selon vous cette protéine présente-elle une activité constitutive résiduelle ? (2 points)
- 3) Proposer un schéma de l'allèle Rosa26R-eYFP. Décrire en quelques lignes la démarche qui permet d'obtenir un tel allèle. (2 points)
- 4) Proposer une représentation des figures S4 et S6, avec les légendes correspondantes. (2 points)
- 5) Expliquer le concept de tolérance centrale. Quel est le rôle des cellules épithéliales thymiques ? (2 points)
- 6) Les auteurs utilisent dans cet article une stratégie de réversion d'un phénotype nul pour Foxn1. Quel est l'intérêt de cette stratégie par rapport à une délétion conditionnelle de ce gène ? (2 points)
- 7) Identifier une question posée par ces résultats et proposer une stratégie expérimentale pour l'étudier. (2 points)

LETTERS

Formation of a functional thymus initiated by a postnatal epithelial progenitor cell

Conrad C. Bleul¹, Tatiana Corbeaux¹, Alexander Reuter¹†, Paul Fisch², Jürgen Schulte Mönting³ & Thomas Boehm¹

The thymus is essential for the generation of self-tolerant effector and regulatory T cells. Intrathymic T-cell development requires an intact stromal microenvironment, of which thymic epithelial cells (TECs) constitute a major part^{1–3}. For instance, cell-autonomous genetic defects of forkhead box N1 (*Foxn1*)⁴ and autoimmune regulator (*Aire*)⁵ in thymic epithelial cells cause primary immunodeficiency and autoimmunity, respectively. During development, the thymic epithelial rudiment gives rise to two major compartments, the cortex and medulla. Cortical TECs positively select T cells⁶, whereas medullary TECs are involved in negative selection of potentially autoreactive T cells⁷. It has long been unclear whether these two morphologically and functionally distinct types of epithelial cells arise from a common bi-potent progenitor cell⁸ and whether such progenitors are still present in the postnatal period. Here, using *in vivo* cell lineage analysis in mice, we demonstrate the presence of a common progenitor of cortical and medullary TECs after birth. To probe the function of postnatal progenitors, a conditional mutant allele of *Foxn1* was reverted to wild-type function in single epithelial cells *in vivo*. This led to the formation of small thymic lobules containing both cortical and medullary areas that supported normal thymopoiesis. Thus, single epithelial progenitor cells can give rise to a complete and functional thymic microenvironment, suggesting that cell-based therapies could be developed for thymus disorders.

The thymus is the primary lymphoid organ that generates a diverse and self-compatible T-cell repertoire. The epithelial component of the thymic stroma is essential for intrathymic T-cell development^{2,3}. In mice homozygous for loss-of-function mutations in the gene encoding the transcription factor *Foxn1*⁹, TECs fail to differentiate^{4,10} and thymopoiesis is completely blocked, causing severe immunodeficiency¹¹. In the normal thymus, TECs found in the cortex and the medulla are functionally distinct. For example, medullary epithelial cells are required for negative selection, failure of which leads to autoimmunity^{5,12,13}. Therefore, TECs might be an attractive source of cell-based strategies to correct or modulate autoimmune disorders⁸.

However, much remains to be learned about their development and function. For instance, an epithelial cell population isolated from an embryonic thymus gives rise to a functional microenvironment consisting of both medullary and cortical compartments when transplanted into ectopic sites^{14,15}, but it is unclear whether this activity resides in one cell type or is the result of the joint activity of many different cell types. Furthermore, it is unclear whether bi-potent progenitors exist in the postnatal thymus. Here, we examine two questions. First, we ask whether cortical and medullary epithelial cell types are derived from one common progenitor and whether such epithelial progenitor cells exist in postnatal thymus tissue. Second, we ask whether single such progenitor cells can give rise

to functionally competent thymic tissue supporting normal thymopoiesis.

To answer the first question, we developed a lineage-tracing procedure based on the *Cre/loxP* system to follow the fate of genetically marked TECs. As a read-out for *Cre* activity we used the well-established *Rosa26R-eYFP* (where eYFP is enhanced yellow fluorescent protein) reporter¹⁶ system that supplies a fluorescent protein only after *Cre*-mediated chromosomal rearrangement at a ubiquitously expressed genomic locus. *Cre* activity was provided by a modified *Cre*-recombinase, driven by the human *K14* promoter (*hK14::Cre-ERT2*) (where ER is human oestrogen receptor)¹⁷. Two features made the latter component particularly attractive for our purpose. First, the *K14* promoter is active in epithelial progenitor cells¹⁸ and so we expected that it might be active also in thymic epithelial precursor cells. Second, *Cre-ERT2* exhibits a low level of activity even in the absence of tamoxifen induction (data not shown), effectively creating somatic mosaics in epithelial compartments.

Although no yellow cells were found in the thymic lobes of newborn (postpartum day zero, P0) *hK14::Cre-ERT2;Rosa26R-eYFP* mice ($n = 10$), about half the mice (15/29) contained yellow cells in the thymic epithelial compartment at P14 (Supplementary Table S1). As mice grew older, the proportion of mice with yellow TECs steadily increased, as did the number of yellow cells per thymus. However, at P14, the number of marked cells per thymus was low, ranging from 3 to 146 cells per total thymus and thus comprised only a minor fraction ($\ll 0.1\%$) of TECs (Supplementary Table S1). In thymus tissue, yellow cells were found to be clustered rather than evenly distributed. Indeed, the observed distribution of yellow cells per unit volume (that is, per section), each comprising about 1–2% of thymic tissue, is incompatible with a Poisson distribution expected for random distribution (Supplementary Table S1, $P < 0.001$, Sign test). This indicated that yellow cells did not arise independently and that cell clusters were the result of single recombination events occurring in cells with proliferative potential.

Of the 58 thymic lobes derived from the 29 animals that we completely sectioned, 21 circumscribed areas (clusters) contained yellow cells; nine single cells were also found (Supplementary Fig. S1a). Four cell clusters occurred in the medulla, each without evidence of associated cortical cells (Fig. 1a; Supplementary Fig. S1); these clusters are reminiscent of the medullary islets described earlier¹⁹ and their observation provides independent evidence for a medullary epithelial progenitor cell. In ten instances, yellow cells occurred only in the cortex but not in the medulla, and nine of those ten instances consisted of a single cell only (Fig. 1b; Supplementary Fig. S1). One cortical cluster was observed (Fig. 1c), consisting of cells arranged concentrically around a medullary islet. This finding is compatible with the existence of a dedicated cortical progenitor cell.

¹Department of Developmental Immunology, Max-Planck Institute of Immunobiology, Stuebeweg 51, D-79108 Freiburg, Germany. ²Department of Pathology, University of Freiburg, Breisacher Strasse 115a, D-79110 Freiburg, Germany. ³Institute of Medical Biometry and Informatics, University of Freiburg, Stefan-Meier-Strasse 26, D-79104 Freiburg, Germany. †Present address: Department of Biology, University of Konstanz, D-78457 Konstanz, Germany.

Sixteen of 21 cell clusters (76%) contained cells of both cortical and medullary phenotypes spanning the cortico-medullary junction (Fig. 1d). These patterns suggest that TEC progenitors exhibiting yellow fluorescence after Cre-mediated recombination at the *Rosa26* locus give rise to groups of genetically related progeny that are found in close proximity to each other. Indeed, mathematical modelling reproduces the appearance of clustered progeny from single progenitors and the results indicate that biologically meaningful parameters for proliferation probabilities of progenitor and differentiated cells and generation times can explain the observed patterns (Supplementary Information and Table S2). Interestingly, the distribution of labelled progeny derived from eYFP-positive/MHC class-II-positive embryonic day (E)12.5 embryonic TECs added to reaggregates of thymic tissue and transplanted into ectopic sites is strikingly similar to the pattern observed in the postnatal lineage tracing experiment (Supplementary Fig. S2). This is compatible with the notion that the differentiation of embryonic and postnatal TECs follows similar rules.

Collectively, the above analyses strongly suggested the presence of bi- and uni-potent progenitor cells for the cortical and medullary compartments, respectively. However, owing to the experimental design of creating somatic mosaics, it was impossible to obtain proof for the functional competence of such progenitors beyond their morphological and immunohistochemical characteristics. We therefore devised a genetic test to examine the proposed differentiation model in functional terms. The design of this experiment was based on the assumption that *Foxn1*-deficient TECs are maintained in an undifferentiated state in the alymphoid rudiment^{4,10}.

We sought to create a null allele of *Foxn1* that could be reverted to the wild-type configuration upon the action of Cre recombinase. Owing to the unique properties of the *hK14::Cre-ERT2* transgene described above, we expected to be able to examine the functional consequences arising from the reversion of *Foxn1* in single epithelial cells within a *Foxn1*-deficient epithelial rudiment. We first confirmed that the *hK14::Cre-ERT2* transgene was also active in *Foxn1*^{-/-}

epithelial cells using mice transgenic for *hK14::Cre-ERT2* and *Rosa26R-lacZ*²⁰ on the *Foxn1*-deficient *nu/nu* background (Fig. 2a). In the thymic rudiment of *hK14::Cre-ERT2;Rosa26R-lacZ;nu/nu* mice, expression of β -galactosidase was confined to rare, often single, cells in an entire rudiment, indicating that Cre-mediated recombination occurred as a singular event. Thus, for subsequent experiments using the *hK14::Cre-ERT2* transgene, differentiated progeny of reverted epithelial cells could be expected to originate from single TEC.

The revertible allele of *Foxn1* was created by insertion of a cassette containing splice acceptor and polyadenylation sites into the intron between exons 6 and 7 of the mouse *Foxn1* gene (Fig. 2b). This insertion was modelled according to a rat *nude* allele²¹ to corrupt the normal splicing process. The formation of truncated non-functional messenger RNAs ultimately resulted in a *nude* phenotype in mice homozygous for this allele (Supplementary Fig. S3a). Excision of the cassette by Cre recombinase was expected to restore normal splicing; indeed, a wild-type phenotype was observed after deletion of the cassette in the germ-line (Supplementary Fig. S3b, c). When mice homozygous for the *Foxn1*^{SA2} allele were made transgenic for the *hK14::Cre-ERT2* construct, peripheral T cells could be detected (Fig. 2c) in a progressively larger proportion of the mice with increasing age. For instance, in one cohort, at 4 weeks of age, 8/18 mice had peripheral T cells, and another five became positive within the following month. The presence of peripheral T cells above the background of T cells observed in *nude* mice was absolutely dependent on the presence of the *hK14::Cre-ERT2* transgene, indicating that the *Foxn1*^{SA2} allele itself is not leaky.

Peripheral T cells in the reverters mice, although fewer in number than in wild-type mice, exhibited high surface levels of T-cell receptor (TCR) beta (Fig. 2c), showed a polyclonal T-cell repertoire (Supplementary Fig. S4), upregulated activation markers upon CD3 ϵ cross-linking (Supplementary Fig. S5) and re-established the immune response to a T-cell-dependent antigen (Supplementary Fig. S6), as well as reactivity in mixed lymphocyte reactions (data not

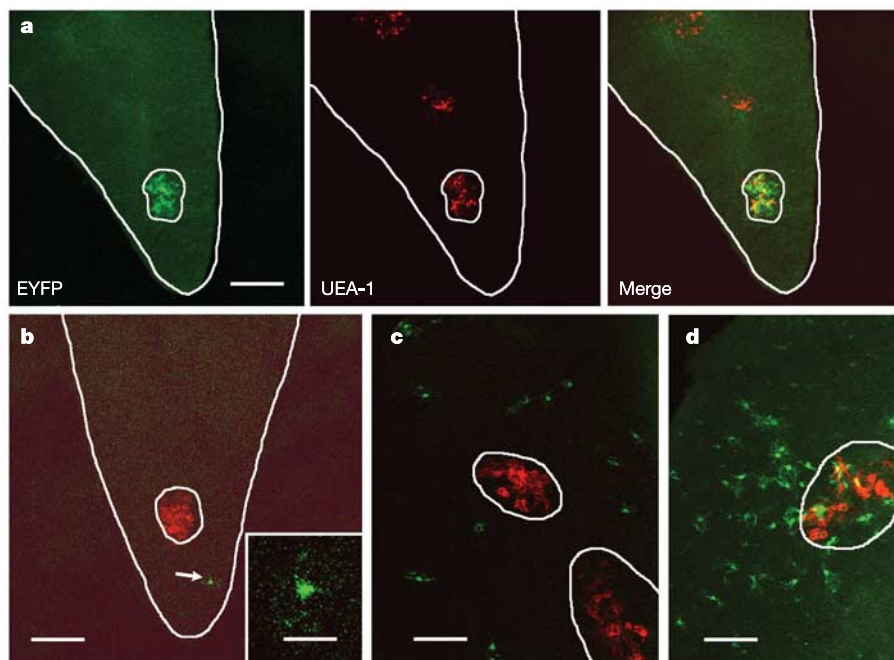


Figure 1 | Examples of cell clusters observed in lineage tracing analysis. **a**, Medullary islet observed via eYFP fluorescence (left); same section stained with UEA-1, which marks a subset of mature medullary cells (middle); merged images of EYFP and UEA-1 (right). Outline of section and genetically marked medullary islet indicated in white. **b**, Single marked

cortical cell (merged images). **c**, Halo of cortical epithelial cells adjacent to medullary islets (red) (merged images). Cortical clusters are more dispersed than medullary islets. **d**, Group of cells spanning the cortico-medullary junction (merged images). Scale bars, 100 μ m (**a**), 100 μ m (**b**), 20 μ m (**b** inset), 50 μ m (**c**), 50 μ m (**d**).

shown). When the thymic rudiment was analysed by histology in such mice, small areas of thymic tissue were apparent adjacent to alymphoid cysts (Fig. 3a). These neo-thymi contained well-defined central medullary areas enclosed by cortical spheres (Fig. 3b) and

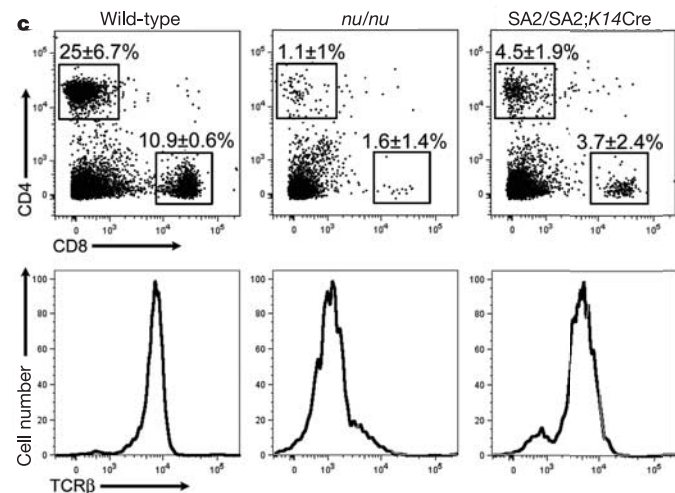
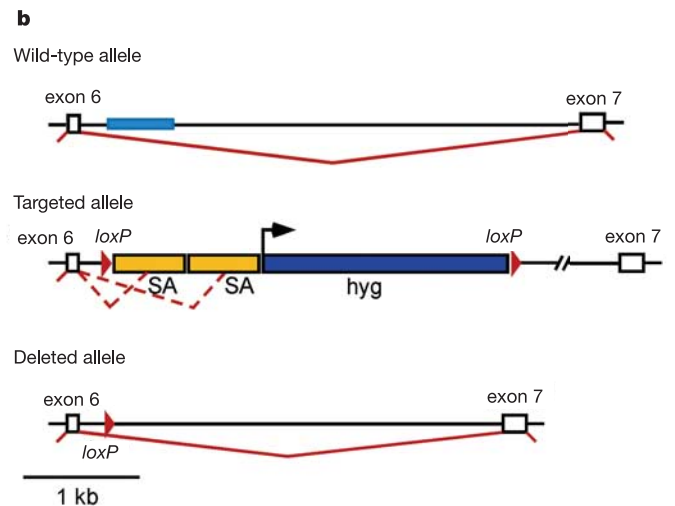
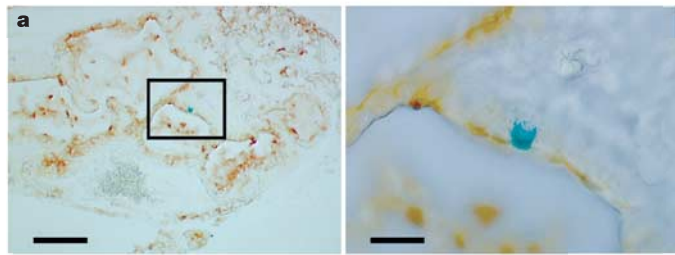


Figure 2 | A revertable *Foxn1* allele (*Foxn1*^{SA2}). **a**, Histological section of thymic rudiment in *hK14::Cre-ERT2;Rosa26R-lacZ;nu/nu* mice stained with an anti-cytokeratin K8 antibody (brownish stain) and developed for β -galactosidase expression (blue stain). Right panel, close-up of the indicated region in the left panel; note the single positive cell in the wall of the cyst. Scale bars, 100 μ m, left panel; 25 μ m, right panel. **b**, Structure of the *Foxn1* locus before (upper line) and after knock-in (middle line) of the SA2 cassette (yellow) and the hygromycin selectable marker (dark blue). Cre-mediated excision of this cassette (bottom line) deletes a small region (indicated by light blue rectangle) in the intron. Red arrowheads, *loxP* sites; splicing pattern indicated by red lines. **c**, Top panels, analysis of splenocytes for CD4-positive and CD8-positive T cells in 8–12-week-old wild-type, nude (*nu/nu*), and *Foxn1*^{SA2}/*Foxn1*^{SA2};*hK14::Cre-ERT2* mice (SA2/SA2;*K14Cre*) (average \pm standard deviation). Bottom panels, surface levels of TCR β for CD4-positive cells.

supported normal T-cell differentiation (Fig. 3c, d; Supplementary Fig. S7a) for at least 21 months (the latest time point examined; Supplementary Fig. S7b). The epithelium in neo-thymi expresses the autoimmune regulator *Aire* and peripheral self antigens (Supplementary Fig. 8), suggesting that central tolerance mechanisms are in place.

Interestingly, no thymic mass consisting of either cortical or medullary epithelium was observed, indicating that to support productive thymopoiesis, the reversion of *Foxn1* function in single cells occurs in a cell type that is positioned upstream of cortical and medullary precursors in the differentiation hierarchy. This experiment shows how epithelial stroma emanating from single progenitor cells gives rise to a microenvironment that supports the immigration, differentiation and emigration of haematopoietic cells. As expected for a cumulative random reversion process, the number and size of

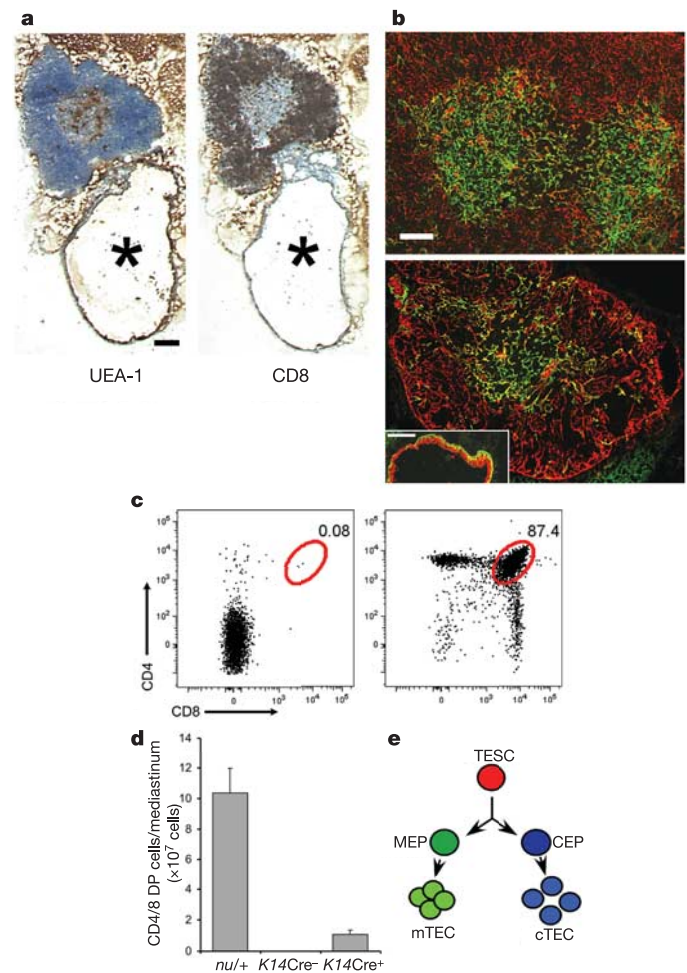


Figure 3 | Postnatal thymopoiesis in *Foxn1*^{SA2}/*Foxn1*^{SA2};*hK14::Cre-ERT2* mice. **a**, Histological section of neo-thymus stained with UEA-1 (left) and anti-CD8 (right). **b**, Anti-cytokeratin K5 (green, specific for medullary TECs) and anti-cytokeratin K8 (red, specific for cortical TECs) staining; cystic rudiment (inset). K5/K8-double positive cells appear yellow. Scale bars, 100 μ m. **c**, Analysis of lymphocytes from the mediastinum of a *Foxn1*^{SA2}/*Foxn1*^{SA2} seven-week-old control mouse (left) and a *Foxn1*^{SA2}/*Foxn1*^{SA2};*hK14::Cre-ERT2* littermate (right). The double-negative cells in the left panel are B cells. **d**, Enumeration of CD4/CD8-double-positive cells in the mediastinum of 7–10-week-old *Foxn1*^{SA2}/*Foxn1*^{SA2} mice with or without the *hK14::Cre-ERT2* (*K14Cre*) transgene; control, *nu/+* mice (average \pm standard deviation). **e**, Proposed scheme of TEC differentiation. A bi-potent progenitor of cortical and medullary epithelium (TESC, thymic epithelial stem cell) gives rise to distinct intermediary progenitor cells (MEP, medullary epithelial progenitor; CEP, cortical epithelial progenitor) and finally to mature medullary and cortical TECs (mTECs and cTECs).

thymic lobules observed in thymic rudiments increased in older mice (Supplementary Fig. S9a); furthermore, the age of analysed mice correlated with increasing numbers of TECs, CD4/CD8 double-positive thymocytes and peripheral T-cell numbers (Supplementary Fig. 9b, c). We also observed re-growth of hair in progressively larger patches of skin in reverter mice, indicating restoration of hair keratinization as a consequence of normalized *Foxn1* function.

Our results provide answers to a number of key problems in TEC biology. We show that the embryonic and adult TEC compartments contain bi-potent progenitor cells that give rise to TECs with both cortical and medullary phenotypes. Our results confirm the presence of medullary precursors¹⁹ and suggest the presence of an equivalent progenitor for the cortical compartment. We cannot determine the relative proportion of these types of progenitor cells in the postnatal thymus, because the method we use here for their detection depends on the (unknown) relative activity of the transgenic construct supplying Cre activity in the different precursor types. Nevertheless, our findings allow us to propose a differentiation scheme of TECs (Fig. 3e): lineage tracing and genetic reversion analysis both suggest that a *Foxn1*-dependent bi-potent precursor initially gives rise to cortical and medullary precursors which then form small clusters of differentiated progeny. Interestingly, the reversion experiment also indicates that direct interaction of ectoderm with endoderm is not required for full differentiation of adult TECs, because mediastinal thymic rudiments are no longer in contact with the cells of this germ layer. Our results also indicate that the bi-potent TEC progenitor cell expresses *Foxn1*.

A surprising finding was that despite the absence of *Foxn1*, epithelial precursors in thymic rudiments survive into the adult period, because they can be induced postnatally to differentiate normally by re-supply of *Foxn1* function. This finding provides functional proof for earlier suggestions of the presence of an immature epithelium in *Foxn1*-deficient thymic rudiments¹⁰. It also shows how a functional epithelial compartment arising from single progenitor cells is capable of organizing fully competent thymopoietic niches. The supply of *Foxn1* is necessary and sufficient to direct the differentiation of immature epithelial cells into fully mature and functionally competent TECs, so the delivery of *Foxn1* to even single progenitor cells of the cystic epithelial rudiment of human *FOXN1*^{-/-} patients^{22,23} (for instance, through viral vectors) may result in clinically relevant and long-lasting thymopoiesis that bone marrow transplantation failed to achieve²⁴. Our results thus suggest a treatment method for this particular kind of primary immunodeficiency.

The presence of a bi-potent progenitor cell in the embryonic thymic epithelial compartment has been unequivocally demonstrated²⁵; our results indicate that such a progenitor also exists in the postnatal thymus. Further work should focus on the isolation of this rare cell type from adult tissues with the possibility of developing cell-based therapies to modify the outcome of autoimmune disorders in adults.

METHODS

More detailed methods are described in the Supplementary Information.

Mice. The Cre-transgenic mouse strain for the ubiquitous deletion of *loxP*-flanked gene segments (*P_{BI-2}::Cre*; 'Cre-deleter' (ref. 26)) was the kind gift of K. Rajewsky. The Cre reporter strains produced by targeted insertion of *lacZ*²⁰ or eYFP¹⁶ into the *Rosa26* locus were kindly provided by P. Soriano and S. Srinivas, respectively. Mice expressing eYFP in all cells were generated by crossing *Rosa26*-eYFP mice with the Cre-deleter strain. The transgenic mouse line driving a modified Cre-protein (Cre-ERT2) under the control of the *hK14* promoter/enhancer¹⁷ was the kind gift of P. Chambon.

The *Foxn1*^{SA2} knock-in allele was created as follows. The targeting construct was assembled in a step-wise fashion. Into the *Xba*I site of the plox2d plasmid²⁷ that is positioned between two tandemly arranged *loxP* sites we inserted two tandemly arranged copies of a 605-base pair (bp) fragment (one copy of this fragment corresponds to nucleotides (nt) 321 to 925 in GenBank accession number Y08910; ref. 21.) each containing splice acceptor and polyadenylation signal sequences to give plasmid pP4SA3. This fragment is derived from a

transposon insertion into the rat *Foxn1* gene identified in the rat *nu^{tmuN}* strain²¹. A triplicated version of this cassette was inserted into plasmid pKSB22A (a modified plasmid derivative of the λ GET exon-trapping vector²⁸) to give plasmid p22SA3i and we confirmed its desired effect on splicing and polyadenylation after transfection into COS7 cells (data not shown). This indicates that the cassette may be generally useful for the construction of revertable alleles.

Immediately upstream of the downstream *loxP* site of pP4SA3, a 2.1-kilobase (kb) *Bgl*III fragment derived from pHA58 (the kind gift of A. Berns; ref. 29.) encoding a hygromycin resistance cassette was cloned. Two fragments with homologies to the mouse *Foxn1* locus were positioned up- and downstream, respectively, of the two *loxP* sites in the final targeting vector. The upstream short homology arm corresponds to nt 36917 to 39877, and the downstream long homology arm corresponds to nt 40433 to 47098 in GenBank accession number Y12488 (ref. 30). The final targeting construct (pP4SA2Whn) contains a deletion of 555 bp of intronic sequence between exon 6 (occurring at nt 39555 to 39651 in GenBank accession number Y12488) and exon 7 (occurring at nt 43958 to 33156 in GenBank accession number Y12488) of the *Foxn1* gene to facilitate the detection of Cre-mediated removal of the SA2-hyg cassette (Fig. 2b). This vector was linearized with *Xho*I and electroporated into R1 embryonic stem cells. Hyg-resistant cells were screened for homologous recombination by Southern blotting using *Bam*HI-digested DNA and a probe derived from exon 3 of *Foxn1* (nt 34186 to 34467); the wild-type allele corresponds to 18.2 kb, the targeted allele to about 11 kb. Several correctly targeted clones were injected into blastocysts, and the chimaeras backcrossed to C57BL/6 mice for germline transmission.

Heterozygous mice were intercrossed to yield homozygous mutant mice and their phenotype analysed as described⁴; as expected, the knock-in allele was allelic to the *nu* allele (data not shown) and indistinguishable in phenotype (Supplementary Fig. S3). It was concluded that the *Foxn1*-SA2hyg knock-in allele (henceforth designated *Foxn1*^{SA2}) represents a null allele of *Foxn1*. To confirm the functionality of the *loxP* sites, these mice were crossed to the Cre-deleter strain; the phenotype of mice homozygous for the deleted allele was normal (Supplementary Fig. S3).

Characterization of TECs in lineage tracing experiments. Fluorescence signals emanating from eYFP-expressing cells and from immunohistochemical stains (UEA-1; K8; MTS-10) were recorded in tissue slices (50 μ m) using a Leica TCS SP2 UV confocal microscope system. Background fluorescence was distinguished from eYFP fluorescence using Leica Spectral Dye Separation software. The average diameter of clusters composed of yellow cells was found to be $160 \pm 115 \mu$ m (average \pm standard deviation); accordingly, we required a minimum distance of about 3 s.d. (= 350 μ m) between aggregates of yellow cells to designate them as independent; the minimum number of cells required per cluster is 1.

Differentiation potential of embryonic TECs. To determine the long-term repopulation potential of embryonic TECs, isolated thymic lobes from E12.5 embryos of the fully recombined *Rosa26*-eYFP strain were dispersed into single cell suspensions¹² and stained with antibodies against CD45 and MHC class II. MHC-class-II-positive, CD45-negative, eYFP-positive cells were sorted into wells of microtitre plates that contained 2×10^5 cells from dissociated E14.5 thymic lobes of BALB/c wild-type mice. The cell suspensions were reaggregated for 2 days and then transplanted under the kidney capsule of BALB/c nude mice. After 5 months, recipient mice were killed and grafts examined for the presence of eYFP-positive cells in the ectopic thymic tissue.

Received 17 January; accepted 26 April 2006.

- Boehm, T., Bleul, C. C. & Schorpp, M. Genetic dissection of thymus development in mouse and zebrafish. *Immunol. Rev.* **195**, 15–27 (2003).
- Anderson, G. & Jenkinson, E. J. Lymphostromal interactions in thymic development and function. *Nature Rev. Immunol.* **1**, 31–40 (2001).
- Gray, D. H. *et al.* Controlling the thymic microenvironment. *Curr. Opin. Immunol.* **17**, 137–143 (2005).
- Nehls, M. *et al.* Two genetically separable steps in the differentiation of thymic epithelium. *Science* **272**, 886–889 (1996).
- Anderson, M. S. *et al.* Projection of an immunological self shadow within the thymus by the aire protein. *Science* **298**, 1395–1401 (2002); published online 10 October 2002 (doi: 10.1126/science.1075958).
- Hogquist, K. A. & Bevan, M. J. The nature of the peptide/MHC ligand involved in positive selection. *Semin. Immunol.* **8**, 63–68 (1996).
- Kyewski, B., & Derbinski, J. Self-representation in the thymus: an extended view. *Nature Rev. Immunol.* **4**, 688–698 (2004).
- Blackburn, C. C. *et al.* One for all and all for one: thymic epithelial stem cells and regeneration. *Trends Immunol.* **23**, 391–395 (2002).
- Nehls, M., Pfeifer, D., Schorpp, M., Hedrich, H. & Boehm, T. New member of the winged-helix protein family disrupted in mouse and rat nude mutations. *Nature* **372**, 103–107 (1994).

10. Blackburn, C. C. *et al.* The nu gene acts cell-autonomously and is required for differentiation of thymic epithelial progenitors. *Proc. Natl Acad. Sci. USA* **93**, 5742–5746 (1996).
11. Cunningham-Rundles, C. & Ponda, P. P. Molecular defects in T- and B-cell primary immunodeficiency diseases. *Nature Rev. Immunol.* **5**, 880–892 (2005).
12. Boehm, T., Scheu, S., Pfeffer, K. & Bleul, C. C. Thymic medullary epithelial cell differentiation, thymocyte emigration, and the control of autoimmunity require lympho-epithelial cross talk via LTbetaR. *J. Exp. Med.* **198**, 757–769 (2003).
13. Akiyama, T. *et al.* Dependence of self-tolerance on TRAF6-directed development of thymic stroma. *Science* **308**, 248–251 (2005); published online 10 February 2005 (doi: 10.1126/science.1105677).
14. Bennett, A. R. *et al.* Identification and characterization of thymic epithelial progenitor cells. *Immunity* **16**, 803–814 (2002).
15. Gill, J., Malin, M., Hollander, G. A. & Boyd, R. Generation of a complete thymic microenvironment by MTS24(+) thymic epithelial cells. *Nature Immunol.* **3**, 635–642 (2002); advance online publication 17 June 2002 (doi:10.1038/ni812).
16. Srinivas, S. *et al.* Cre reporter strains produced by targeted insertion of EYFP and ECFP into the ROSA26 locus. *BMC Dev. Biol.* **1**, 4 (2001); published online 27 March 2001 (doi: 10.1186/1471-213x-1-4).
17. Li, M. *et al.* Skin abnormalities generated by temporally controlled RXRalpha mutations in mouse epidermis. *Nature* **407**, 633–636 (2000).
18. Vassar, R., Rosenberg, M., Ross, S., Tyner, A. & Fuchs, E. Tissue-specific and differentiation-specific expression of a human K14 keratin gene in transgenic mice. *Proc. Natl Acad. Sci. USA* **86**, 1563–1567 (1989).
19. Rodewald, H. R., Paul, S., Haller, C., Bluethmann, H. & Blum, C. Thymus medulla consisting of epithelial islets each derived from a single progenitor. *Nature* **414**, 763–768 (2001).
20. Soriano, P. Generalized lacZ expression with the ROSA26 Cre reporter strain. *Nature Genet.* **21**, 70–71 (1999).
21. Huth, M., Schlake, T. & Boehm, T. Transposon-induced splicing defect in the rat nude gene. *Immunogenetics* **45**, 282–283 (1997).
22. Adriani, M. *et al.* Ancestral founder mutation of the nude (FOXP1) gene in congenital severe combined immunodeficiency associated with alopecia in southern Italy population. *Ann. Hum. Genet.* **68**, 265–268 (2004).
23. Frank, J. *et al.* Exposing the human nude phenotype. *Nature* **398**, 473–474 (1999).
24. Pignata, C. *et al.* Human equivalent of the mouse Nude/SCID phenotype: long-term evaluation of immunologic reconstitution after bone marrow transplantation. *Blood* **97**, 880–885 (2001).
25. Rossi, S. W., Jenkinson, W. E., Anderson, G. & Jenkinson, E. J. Clonal analysis reveals a common progenitor for thymic cortical and medullary epithelium. *Nature* doi:10.1038/nature04813 (this issue).
26. Schwenk, F., Baron, U., & Rajewsky, K. A cre-transgenic mouse strain for the ubiquitous deletion of loxP-flanked gene segments including deletion in germ cells. *Nucleic Acids Res.* **23**, 5080–5081 (1995).
27. Nehls, M., Messerle, M., Sirulnik, A., Smith, A. J. & Boehm, T. Two large insert vectors, lambda PS and lambda KO, facilitate rapid mapping and targeted disruption of mammalian genes. *Biotechniques* **17**, 770–775 (1994).
28. Nehls, M., Pfeifer, D., Micklem, G., Schmoor, C. & Boehm, T. The sequence complexity of exons trapped from the mouse genome. *Curr. Biol.* **4**, 983–989 (1994).
29. te Riele, H., Maandag, E. R., Clarke, A., Hooper, M. & Berns, A. Consecutive inactivation of both alleles of the *pim-1* proto-oncogene by homologous recombination in embryonic stem cells. *Nature* **348**, 649–651 (1990).
30. Schorpp, M., Hofmann, M., Dear, T. N. & Boehm, T. Characterization of mouse and human nude genes. *Immunogenetics* **46**, 509–515 (1997).

Supplementary Information is linked to the online version of the paper at www.nature.com/nature.

Acknowledgements We thank A. Maul-Pavicic, S. Groß, C. Sainz-Rueda, A. Haas-Assenbaum, C. Happe, E. Nikolopoulos and M. Konrath for help during various stages of this project, and K. Rajewsky, P. Soriano, P. Chambon, S. Srinivas, K. Eichmann, G. Turchinovich, for mouse lines or reagents. This work was supported by grants from the Deutsche Forschungsgemeinschaft and the Max-Planck Society.

Author Information Reprints and permissions information is available at npg/nature.com/reprintsandpermissions. The authors declare no competing financial interests. Correspondence and requests for materials should be addressed to T.B. (boehm@immunbio.mpg.de).

Figure S1 | Characterization of genetically marked epithelial cells observed in lineage tracing analysis. **a**, Schematic of five potential patterns indicated in a thymus with two medullary areas, symbolized by two small circles. A single medullary cell (top left) was not observed; in four instances, medullary clusters (middle left) were observed (cluster size indicated in brackets; range 12 to 65 cells); in nine instances, single cortical cells (top right) were observed and in one instance, a cluster consisting of a total of 32 cells was observed to occur in three consecutive 50 μ m sections (one section shown in Fig. 1c). The majority of clusters (16/21), consisted of medullary and cortical cells (bottom left; range 11 to 85). **b**, **c**, Morphological characteristics of TECs expressing cytoplasmic EYFP protein. **b**, Single cortical epithelial cell. **c**, Medullary islet. Note the extensive reticular network emanating from the central body of the cortical cell, whereas the extensions of medullary cells appear more blunted. Scale bars, 10 μ m. **d**, Immunohistological analysis of TECs expressing cytoplasmic EYFP protein. Cortical cells are positive for K8 (upper panels), medullary epithelial cells are positive for MTS10 (lower panels). Scale bars, 10 μ m.

Figure S2 | Evidence for common cortico-medullary progenitors in E12.5 thymus. MHC class II-positive epithelial cells (previously shown to contain epithelial progenitor cells⁸⁻¹⁰) were dissociated from E12.5 thymi of fully recombined Rosa26-EYFP transgenic mice. About 15,000 cells were then reaggregated with epithelial cells from E14.5 non-transgenic mice and transplanted under the kidney capsule of *nude* mice. After 5 months, the resulting ectopic thymi were examined for the

presence of yellow-fluorescent cells. In each of these cases, yellow cells were contained in a single circumscribed region of the large thymic tissue that contained cells with immunohistological and morphological hallmarks of both medullary (medullary islet encircled) and cortical epithelial cells, suggesting that they arose from a single precursor cell. The pattern became multi-focal with a higher input of yellow cells. The unknown clonogenicity of yellow epithelial cells in these experiments precluded a numerical assessment of precursor frequency in E12.5 thymic epithelial cells. Nevertheless, the striking similarity in the spatial arrangement of TECs in this and the lineage tracing experiments (c.f. Fig. 1d) suggested that differentiation of embryonic and postnatal TECs follows similar rules. Scale bar, 50 μ m.

Figure S3 | Characterization of *Foxn1*^{SA2}/*Foxn1*^{SA2} mice. **a**, External appearance. Note the lack of a normal hair coat similar to *nu/nu* mice. **b**, **c**, Reversion of the *Foxn1*^{SA2} allele via Cre-mediated excision in early development. **b**, Schematic of wild-type and deleted alleles (c.f. Fig. 2) with the position of screening primers CB313 and CB314 indicated. **c**, PCR assay for genomic configuration of the *Foxn1* locus. The wild-type amplicon is 752, the amplicon arising from the deleted allele is 231 bp in size. Results are shown for genomic DNA isolated from tail tissue of mice with the following genotypes: lane 1, wild-type (+/+) control; lane 2, *Foxn1*^{SA2}/*Foxn1*^{SA2}//P_{Bi-2}::Cre (Ref. ¹¹); lane 3, *Foxn1*^{SA2}/+//P_{Bi-2}::Cre. This analysis indicates that the SA2 cassette can be efficiently removed from and reconstitutes the *Foxn1* locus. Molecular weight (MW) marker is a 100bp ladder, with the 600bp band indicated. **d**, FACS analysis of thymocytes isolated from the thymus of the mouse shown in lane 2 in **c**, indicating that normal thymopoiesis occurs after excision of the SA2-

cassette; the hair coat of this mouse is also normal (not shown). The percentage of cells in the indicated gates is shown.

Figure S4 | Normal diversity of TCRs in

Foxn1^{SA2}/Foxn1^{SA2}//hK14::Cre-ERT2 mice. **a**, Usage of V β chains in splenic CD4 single-positive T cells of Foxn1^{SA2}/Foxn1^{SA2}//hK14::Cre-ERT2 mice. The results for five individual mice of 7-12 week of age are indicated by different colors. Usage of different V β -chains in peripheral CD4-positive T cells was determined by FACS analysis using specific monoclonal antibodies. Values observed in age-matched *nu/+* mice are indicated by red bars. **b**, Spectratyping analysis for the indicated V β gene families (12 week old mice) indicating that *nu/nu* mice have a highly skewed repertoire, whereas that in Foxn1^{SA2}/Foxn1^{SA2}//hK14::CreERT2 approaches that of normal mice. Qualitatively similar results were obtained for V β 1, V β 3.1, V β 6, V β 7, V β 8.1, V β 11, V β 13, V β 20 families (data not shown). **c**, Sequence diversity of CDR3 regions in TCR β cDNAs (12 week old mice) with V β 8 variable regions. The results for two individual mice for each of the three indicated genotypes are shown. The percentage of unique sequences among analyzed cDNAs (number indicated below columns) is shown. All wild-type sequences were unique (100% singlets); *nude* mice have an oligoclonal repertoire, with a low proportion of singlets among the sequenced cDNAs; Foxn1^{SA2}/Foxn1^{SA2}//hK14::Cre-ERT2 mice have a near normal diversity that is significantly different from that of *nude* mice (t-test, two-tailed)

Figure S5 | Characterization of splenocytes in

Foxn1^{SA2}/Foxn1^{SA2}//hK14::Cre-ERT2 mice. **a**, Surface phenotype of splenocytes from 8 week old mice. Wild-type mice have a lower proportion of activated (CD44^{high}, CD62L^{low}, CD25^{high}) peripheral T cells

than Foxn1^{SA2}/Foxn1^{SA2}//hK14::Cre-ERT2 mice, consistent with homeostatic proliferation of T cells emanating from neo-thymi in reverter mice (results shown for CD4 subset). **b**, Activation of splenic T cells by anti-CD3 ϵ treatment in vitro. Despite initially increased levels of activation markers, T cells from Foxn1^{SA2}/Foxn1^{SA2}//hK14::Cre-ERT2 mice can nevertheless be stimulated by CD3 ϵ cross-linking, as indicated by further up-regulation of CD44 and CD25. Histogram plots are gated on CD4-positive splenocytes that have been incubated for four days in either anti-CD3 ϵ coated wells (bold line) or PBS-control wells (thin line).

Figure S6 | T-dependent immune response in

Foxn1^{SA2}/Foxn1^{SA2}//hK14::Cre-ERT2 mice. IgG1 response against the hapten nitrophenol coupled to chicken γ -globulin (CG-NP). This response is strictly dependent on functional T cells and thus shows the restoration of T cell function in Foxn1^{SA2}/Foxn1^{SA2}//hK14::Cre-ERT2 (abbreviated K14Cre+) but not Foxn1^{SA2}/Foxn1^{SA2} (abbreviated K14Cre-) mice. Each data point represents one mouse.

Figure S7 | Normal thymopoiesis in Foxn1^{SA2}/Foxn1^{SA2}//hK14::Cre-ERT2 mice. **a**, FACS analysis of total thymocytes (top panels), double-negative immature thymocytes (middle panels) and mature CD4-positive thymocytes (lower panels). T cells expressing the γ/δ TCR and NKT cells were also found (data not shown). **b**, Sustained thymopoiesis in 21 month old Foxn1^{SA2}/Foxn1^{SA2}//hK14::Cre-ERT2 mice. Analysis of CD4 and CD8 markers on thymocytes (top panel) indicates ongoing thymopoiesis. Splenocytes of the same mouse contain a large proportion of T cells (middle panel), with high levels of TCR β surface expression (shown for CD4-positive cells, bottom panel). The pattern of activation markers

(CD44, CD69, CD25, CD62L) in such mice is similar to 8 week old mice (not shown).

Figure S8 | Evidence for the expression of *Aire* and peripheral self-antigens in thymic epithelial cells of $\text{Foxn1}^{\text{SA2}}/\text{Foxn1}^{\text{SA2}}//\text{hK14}::\text{Cre-ERT2}$ mice. a, FACS profile of CD45-negative EpCAM-positive thymic epithelial cells present in neo-thymi of reverter mice; the cells in the indicated gate were sorted for subsequent RNA isolation. **b**, Expression profile of TECs isolated as in **a** as determined by RT-PCR. The results for the auto-immune regulator *Aire* and a representative example of peripheral self antigens (*Gad67*) are shown. The quality of cDNA was controlled by *Hprt* analysis. The fragment sizes of amplicons is indicated on the right. The proportion of thymic $\text{CD4}^+\text{CD25}^+$ T regulatory cells in neo-thymi ($0.39\pm 0.18\%$ (n=6)) is indistinguishable from that of wild-type thymi ($0.3\pm 0.09\%$; n=6).

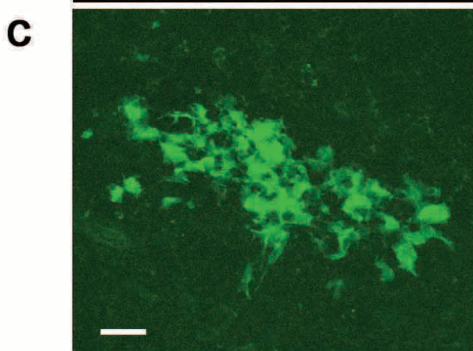
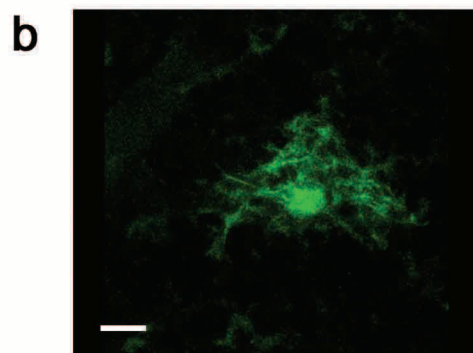
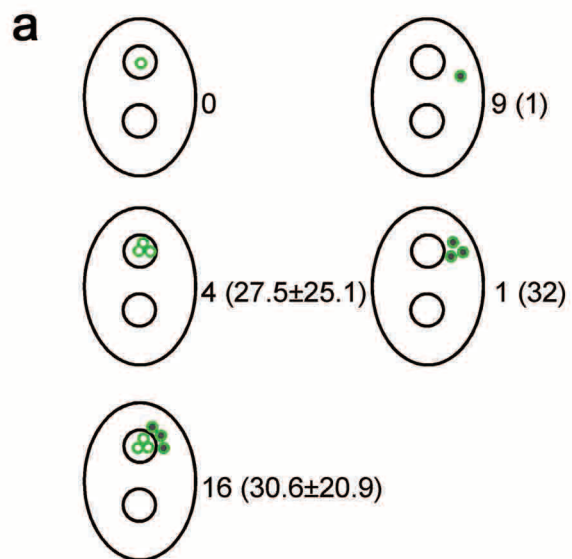
Figure S9 | Thymopoiesis correlates with peripheral T cell reconstitution in $\text{Foxn1}^{\text{SA2}}/\text{Foxn1}^{\text{SA2}}//\text{hK14}::\text{Cre-ERT2}$ mice. a, Histological verification of increased thymopoietic tissue in thymic rudiments over time. The age of mice analysed is indicated at the top, arrows point to neo-thymi, asterisks denote cystic parts of rudiments. In older mice, medullary regions tend to coalesce into larger areas (data not shown). **b**, The number of EpCAM-positive thymic epithelial cells correlates with the number of CD4/CD8 double-positive thymocytes as determined by FACS analysis after enzymatic digestion of thymic rudiments (average values from 2 mice of the indicated age are shown). **c**, Increasing levels of T cell sub-populations in peripheral blood (left panel)

and spleen (right panel) over time indicating an increasing T cell pool. The results for at least 3 mice per group are shown.

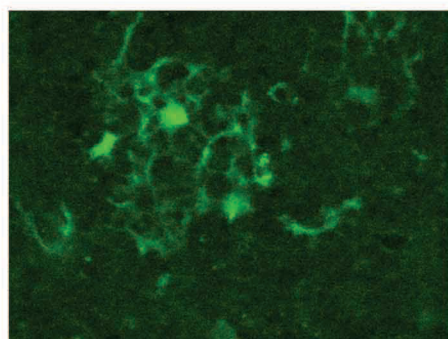
Table S1 | Means and variances of the number of yellow cells in thymic tissues of hK14::Cre-ERT2//Rosa26R-EYFP mice. The characteristic feature of a Poisson (i.e. random) distribution is that the means and variances of the observed parameter are the same. This is not the case here ($P < 0.001$; Sign test), even in the more stringent case of variance equals five-fold of the mean ($P < 0.05$). The number and arrangement of yellow cells was determined by complete sectioning of thymi.

Table S2 | Proliferation probabilities and cluster size. Under the assumptions detailed in Supporting Text for the generation model, biologically meaningful parameters reproduce the observed cluster size. For a cluster of 32 cells, the probability of a progenitor cell to divide has to be about 50%, whereas that of differentiated progeny about 5%.

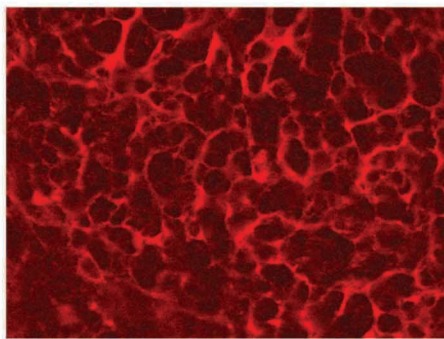
Supplementary Fig. S1



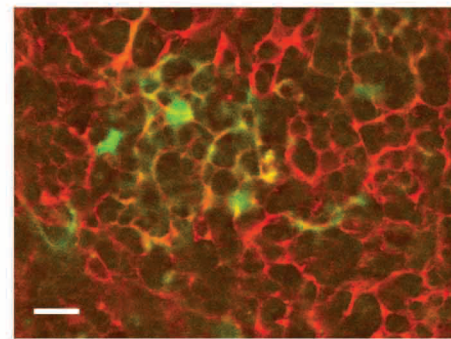
d



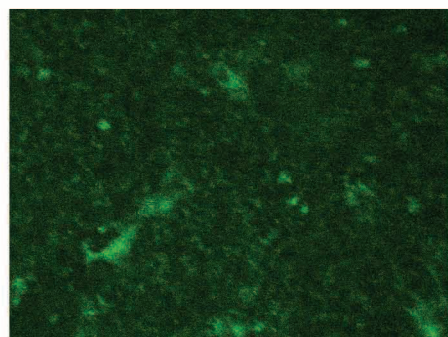
EYFP



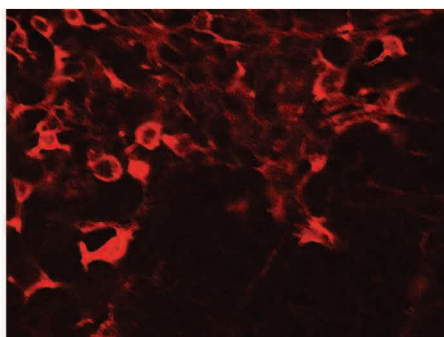
anti-cytokeratin 8



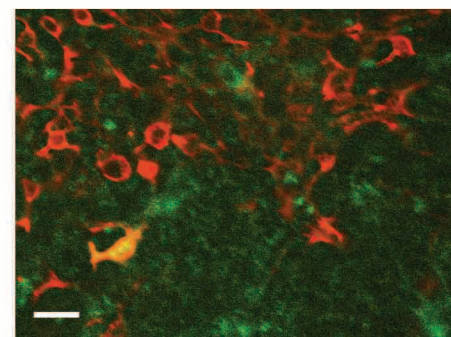
merge



EYFP

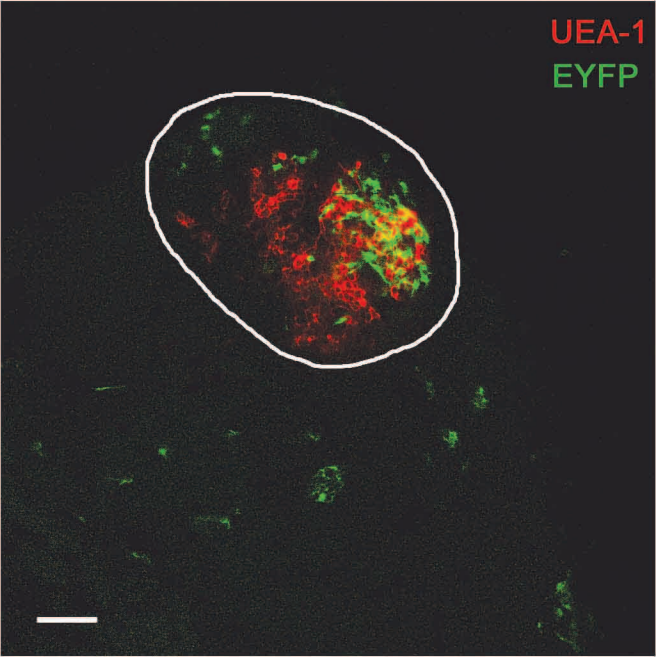


MTS10



merge

Supplementary Fig. S2

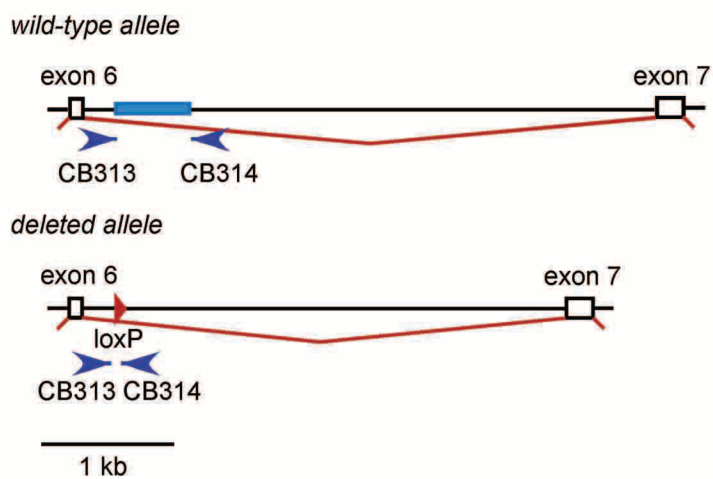


Supplementary Fig. S3

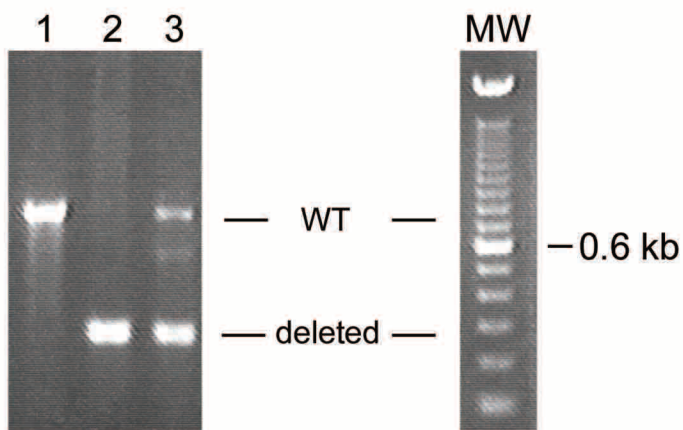
a



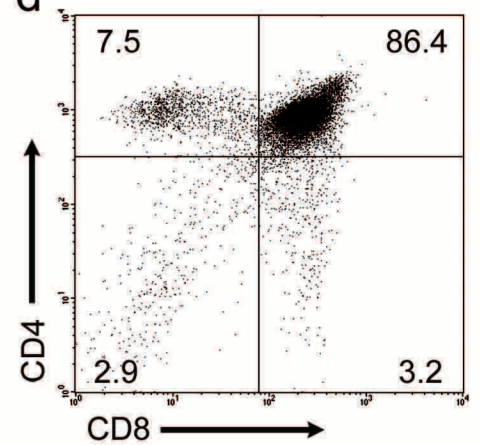
b



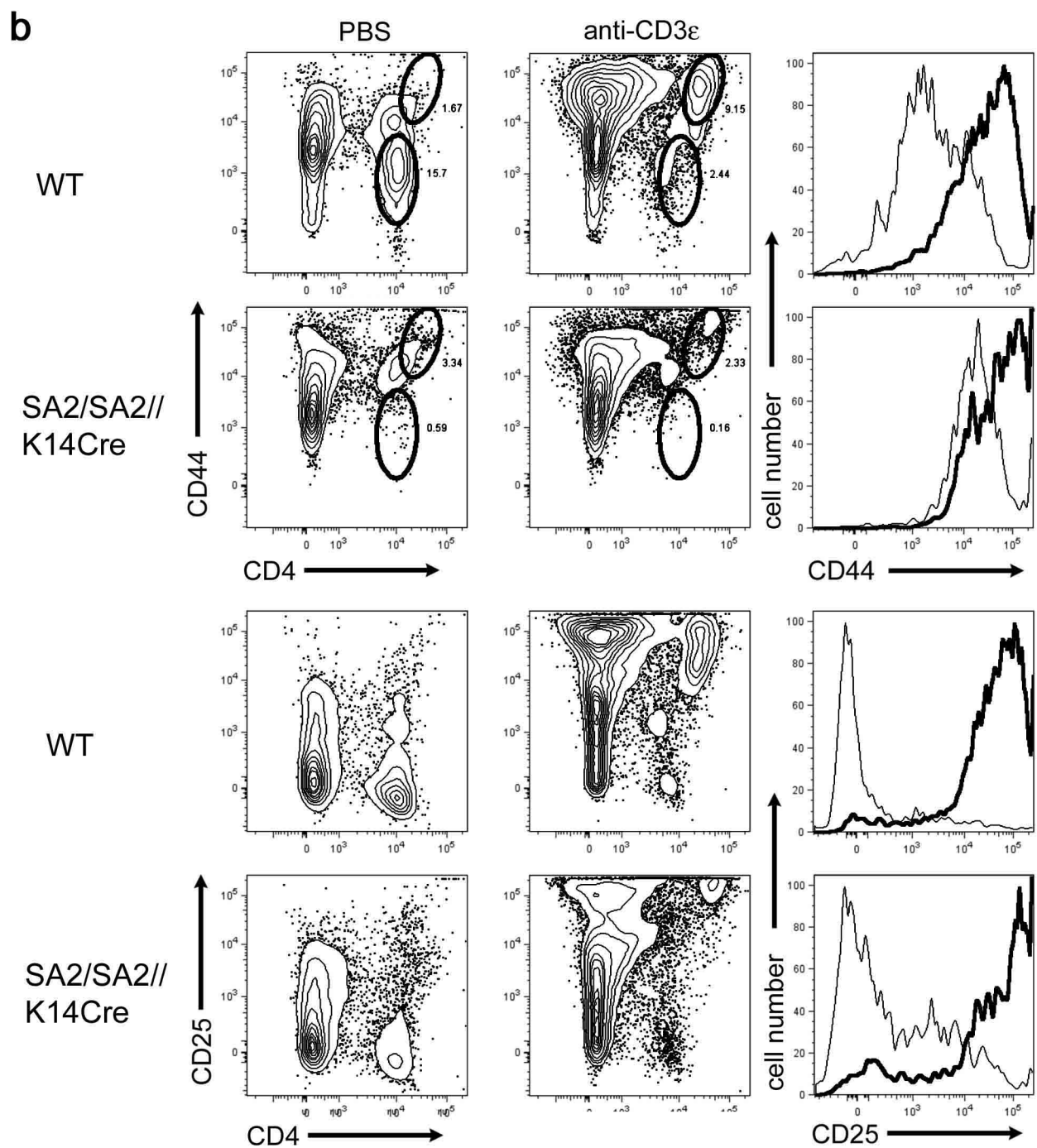
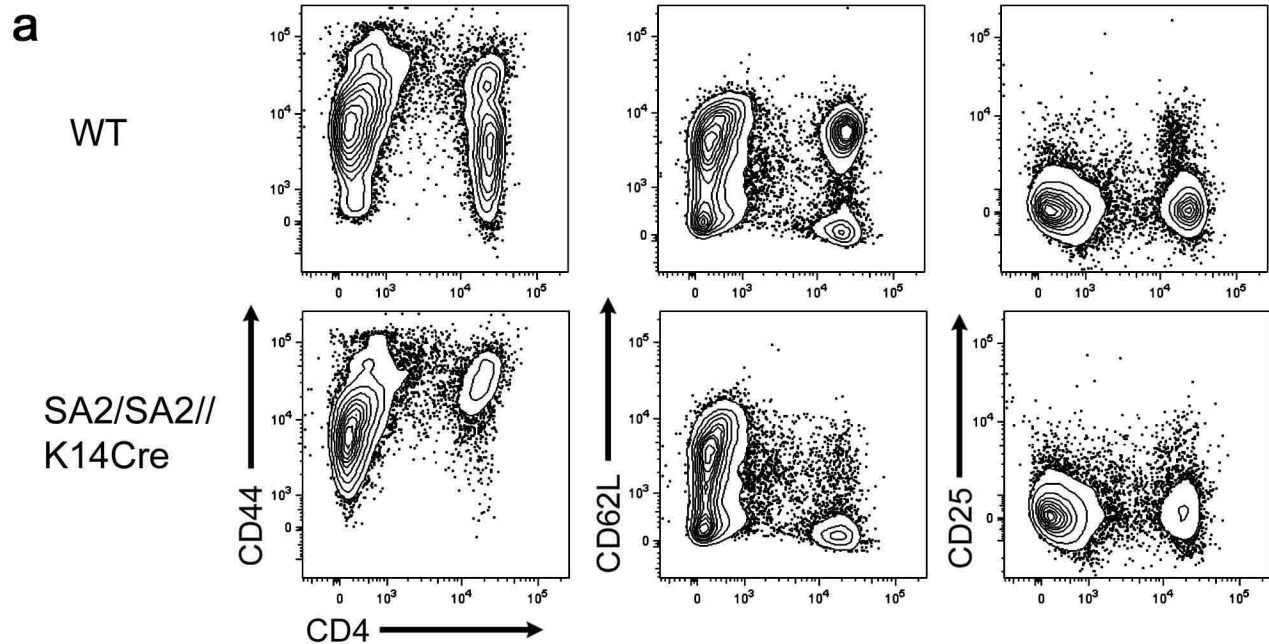
c



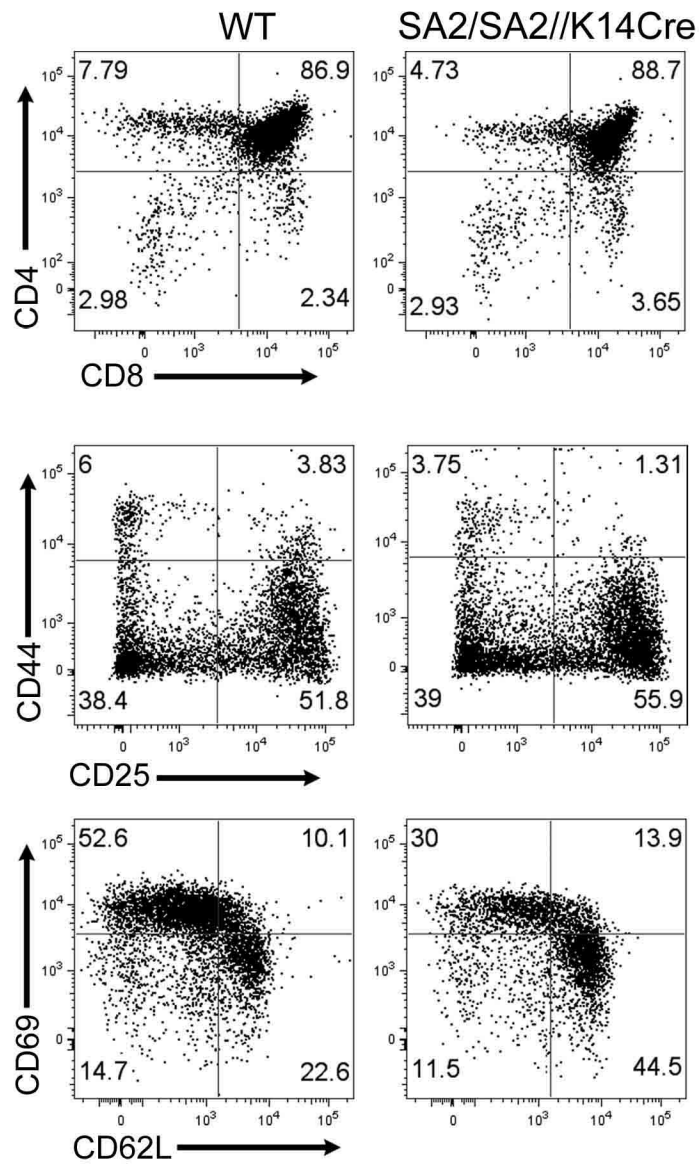
d



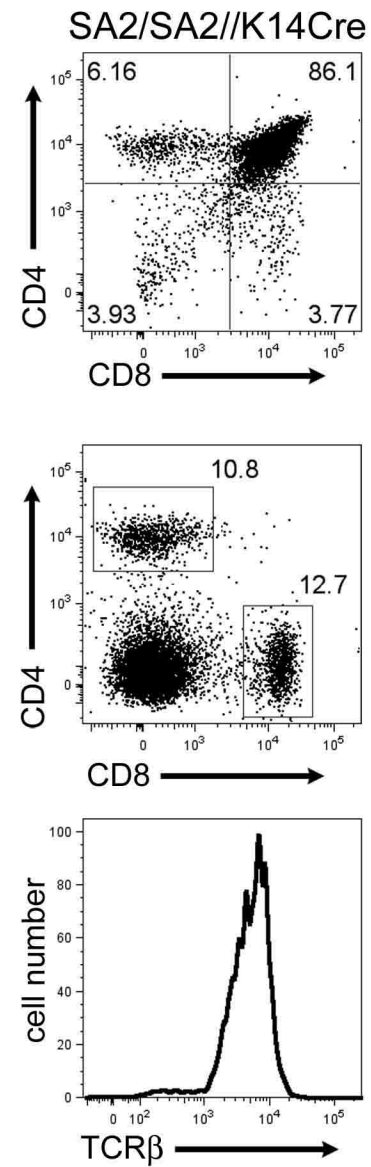
Supplementary Fig. S5



a

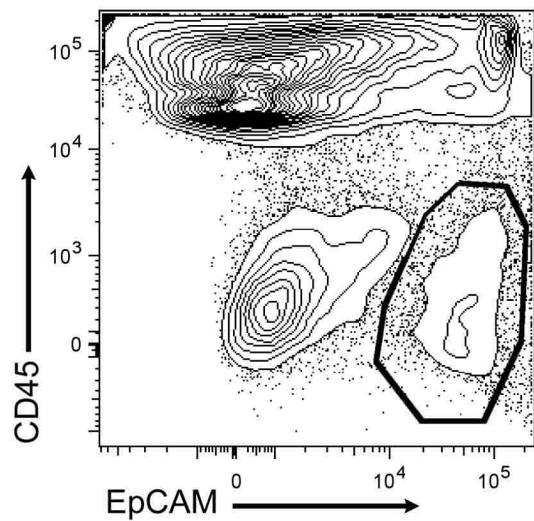


b



Supplementary Fig. S8

a



b

